Published in final edited form as:
Biochemistry. 2012 February 14; 51(6): 1297–1305. doi:10.1021/bi201786s.

Reaction Pathway and Free Energy Profiles for Butyrylcholinesterase- Catalyzed Hydrolysis of Acetylthiocholine

Xi Chen[1,2,a], **Lei Fang**[2,a], **Junjun Liu**[1,2], and **Chang-Guo Zhan**[2,*]

[1]Key Laboratory of Pesticide & Chemical Biology of the Ministry of Education, College of Chemistry, Central China Normal University, Wuhan 430079, P. R. China

[2]Department of Pharmaceutical Sciences, College of Pharmacy, University of Kentucky, 789 South Limestone Street, Lexington, KY 40536

Abstract

The catalytic mechanism for butyrylcholineserase (BChE)-catalyzed hydrolysis of acetylthiocholine (ATCh) has been studied by performing pseudobond first-principles quantum mechanical/molecular mechanical-free energy (QM/MM-FE) calculations on both acylation and deacylation of BChE. Additional quantum mechanical (QM) calculations have been carried out, along with the QM/MM-FE calculations, to understand the known substrate activation effect on the enzymatic hydrolysis of ATCh. It has been shown that the acylation of BChE with ATCh consists of two reaction steps including the nucleophilic attack on the carbonyl carbon of ATCh and the dissociation of thiocholine ester. The deacylation stage includes nucleophilic attack of a water molecule on the carboxyl carbon of substrate and dissociation between the carboxyl carbon of substrate and hydroxyl oxygen of Ser198 side chain. QM/MM-FE calculation results reveal that the acylation of BChE is rate-determining. It has also been demonstrated that an additional substrate molecule binding to the peripheral anionic site (PAS) of BChE is responsible for the substrate activation effect. In the presence of this additional substrate molecule at PAS, the calculated free energy barrier for the acylation stage (rate-determining step) is decreased by ~1.7 kcal/mol. All of our computational predictions are consistent with available experimental kinetic data. The overall free energy barriers calculated for BChE-catalyzed hydrolysis of ATCh at regular hydrolysis phase and substrate activation phase are ~13.6 and ~11.9 kcal/mol, respectively, which are in reasonable agreement with the corresponding experimentally-derived activation free energies of 14.0 kcal/mol (for regular hydrolysis phase) and 13.5 kcal/mol (for substrate activation phase). .

Introduction

Cholinesterases are a family of enzymes that catalyze the hydrolysis of neurotransmitter acetylcholine (ACh), an essential reaction necessary to allow a cholinergic neuron to return to the resting state after impulse transmission. There are two types of cholinesterases, *i.e*. acetylcholinesterase (AChE) and butyrylcholinesterase (BChE), that differ in their distribution in the body. AChE mainly exists in neuromuscular junctions and cholinergic synapses, and hydrolyzes ACh with extremely high efficiency.[1] BChE is known as plasma cholinesterase, which is widely distributed in tissues and plasma. Although the physiological

Correspondence: Chang-Guo Zhan, Ph.D., Professor, Department of Pharmaceutical Sciences, College of Pharmacy, University of Kentucky, 789 South Limestone Street, Lexington, KY 40536, TEL: 859-323-3943, FAX: 859-323-3575, zhan@uky.edu.
[*]Corresponding author. zhan@uky.edu. .
[a]These authors contributed equally to this work.

roles of BChE are still not completely clear, it has been known that BChE can catalyze the hydrolysis of various acyl cholines, acyl thiocholines,[2] cocaine,[3] and acetanilides.[4] It has been noted that BChE can rapidly hydrolyze ACh in the nerves and brain[5-6] and, thus, BChE can apparently substitute for AChE in maintaining the structural and functional integrity of central cholinergic pathway.

In addition, BChE has been proven a therapeutically important protein. First of all, BChE has been used as a bioscavenger in clinic for detoxification of organophosphorus (OP) nerve agents.[7-8] Our recently reported studies[3, 9-22] have led to discovery of high-activity mutants of BChE with a considerably improved catalytic efficiency against naturally-occurring, widely- abused cocaine. The high-activity mutants of BChE have been recognized as promising candidates for therapeutic treatment of cocaine overdose and addiction.[23] In addition, BChE is an important target for cholinergic drugs (that include reversible inhibitors of BChE and/or AChE) in treatment of Alzheimer disease (AD) *etc*.[24]

According to X-ray crystal structures of AChE and BChE reported so far, the overall architecture of BChE is quite similar to that of AChE.[25] The active site of BChE is located at the bottom of deep “aromatic gorge” lined by side chains of several aromatic residues. The channel leading from the surface to the active site is much less confining than that of AChE.[26] Hence, the active site of BChE can accommodate a larger ligand such as cocaine.[10] Similar to AChE, the active site of BChE possesses a catalytic triad (consisting of Ser198, Glu325, and His438) and an oxyanion hole (consisting of Gly116, Gly117, and Ala199) that are essential for the catalytic function. It is commonly accepted that, when a substrate molecule reaches the active site of BChE, the hydroxyl group of Ser198 acts as a nucleophile to attack the carbonyl carbon of the substrate, which initiates the acylation of BChE. The acylation gives an acyl-enzyme intermediate. Subsequently, a water molecule initiates the deacylation to break the ester linkage. Throughout the hydrolysis process, the Glu325-His438 pair is crucial in activating the nucleophile and in transferring a proton to the leaving group and, thus, significantly accelerates the hydrolysis reaction.

Cholinesterase-catalyzed hydrolysis of ACh or acetylthiocholine (ATCh) has been the topic for extensive experimental and computational studies.[1, 27-38] The molecular geometry of ATCh is essentially the same as that of ACh, as the only structural difference between the two substrates is that the ester oxygen (O) in ACh is replaced by a sulfur (S) atom in ATCh. ACh and ATCh were considered to have similar hydrolysis reactions in AChE and BChE, but the experimental assay for the enzyme activity against ATCh is more convenient than that against ACh. Thus, ATCh has widely been used as an “equivalent” substitute of ACh in experimental studies on the AChE/BChE-catalyzed hydrolysis of ACh in the absence/presence of an AChE/BChE inhibitor for mechanistic studies and drug discovery.[2, 5, 37, 39] The kinetic studies have revealed a complex kinetic behavior of the BChE-catalyzed hydrolysis of ATCh.[2, 40-44] At a low ATCh concentration (0 to 0.3 mM, regular hydrolysis phase) the kinetic data fit well to the equation of the standard Michaelis-Menten kinetics, whereas at a high substrate concentration (over 0.3 mM, substrate activation phase) there is a ~3-fold increase in the turnover number (catalytic rate constant k_{cat}) of the BChE enzyme in the presence of excess substrate.[2] This substrate activation is generally considered to be a defining property of BChE, in contrast to AChE which exhibits the substrate inhibition. Masson *et al*. have showed that the Asp70, which is located in the peripheral anionic site of BChE, is essential for the phenomenon of substrate activation.[42] Interestingly, the corresponding residue in AChE, Asp72, has a role in the substrate inhibition in AChE as shown by the finding that Asp72Gly reduced substrate inhibition in AChE.[45] Kinetic study[37] revealed that the reaction rate constant for the deacylation is smaller than that for the acylation, indicating that the deacylation is rate-determining for AChE-catalyzed hydrolysis of ACh. Reported QM/MM studies[36, 38] on AChE-catalyzed hydrolysis of ACh further

suggested that the first reaction step in deacylation is rate-determining for the catalytic hydrolysis process. With respect to the BChE-catalyzed hydrolysis of ACh, early studies suggested that the deacylation could be rate-determining at this stage.[40] However, a series of recent studies demonstrated that at a low substrate concentration, hydrolysis of ACh is rate-determined by the acylation reaction,[2, 41, 46] which is consistent with our recently reported study.[47] Despite extensive studies on the catalytic mechanisms of cholinesterase-catalyzed hydrolysis of ACh/ATCh,[1-2, 15, 27-30, 33-34, 36, 38, 48-50] questions remain for the mechanism of the substrate activation for BChE-catalyzed hydrolysis of ACh/ATCh. For example, what is the main factor leading to the observed substrate activation effect? Does the substrate activation effect change the reaction pathway or the rate-determining step of ACh/ATCh hydrolysis by BChE? In the present study, we have carried out pseudobond first-principles quantum mechanical/molecular mechanical-free energy (QM/MM-FE) calculations[51-54] to study the detailed reaction pathway for BChE-catalyzed hydrolysis of ATCh. The pseudobond first-principles QM/MM-FE approach[51-52, 54-55] has been demonstrated to be a powerful tool in simulating a variety of enzymes,[12, 29-30, 53, 56-57] and some theoretical predictions[29-30] were subsequently confirmed by experimental studies.[58-60] The computational data clearly reveal the detailed reaction pathway and the corresponding free energy profiles for BChE-catalyzed ATCh hydrolysis. The rate-determining steps are thereby identified, and the roles of essential residues including the catalytic triad and oxyanion hole are discussed on the basis of the QM/MM-optimized geometries of the key states in each catalytic hydrolysis reaction process. Based on the QM/MM-FE free energy profile determined for BChE-catalyzed hydrolysis of ATCh, the substrate activation effect was examined and the key factor leading to this phenomenon was identified.

Computational and Experimental Methods

Preparation of the Initial Structures

The initial structures of BChE-ATCh complex (ES) was constructed from the corresponding BChE-ACh complex structure determined in our previous study.[47] Based on the structural similarity between ACh and ATCh, it was believed that the binding mode and hydrolysis mechanism of ATCh should be very similar to those of ACh.[37] For this reason, in the preparation for the calculations on acylation of BChE with ATCh, the initial structure of the ES was constructed by replacing the ester oxygen of substrate with a sulfur atom based on the corresponding QM/MM-optimized ES geometry of BChE with ACh. At the time when the acylation is finished, the thiocholine part of ATCh moves away from the binding site, resulting in the acylated enzyme structure for the ATCh hydrolysis.

Minimum-Energy Path of the Enzymatic Reaction

With a reaction coordinate driving method and an iterative energy minimization procedure,[54] the enzyme reaction path was determined by performing the pseudobond QM/MM calculations at the B3LYP/6- 31+G*:AMBER level, in which the QM calculations were performed at the B3LYP/6-31+G* level of theory by using a modified version of Gaussian03 program[61] and the MM calculations were performed by using a modified version of the AMBER8 program.[62] The reaction coordinate driving method is based on the computational determination of the energy profile along a possible minimum-energy reaction path. The determined energy profile will clearly show the transition state and the corresponding local minimum on the energy surface along the possible reaction path examined. Normal mode analyses were performed to characterize the reactants, intermediates, transition states, and final products. In addition, single-point energy calculations were carried out at the QM/MM(MP2/6-31+G*:AMBER) level on the QM/MM-optimized geometries. Throughout the QM/MM calculations, the boundary carbon atoms were treated with improved pseudobond parameters.[51] No cutoff for non-bonded

interactions was used in the QM/MM calculations. For the QM subsystem, the convergence criterion for geometry optimizations follows the original Gaussian03 defaults. For the MM subsystem, the geometry optimization convergence criterion is when the root-mean-square deviation (rmsd) of energy gradient is less than 0.1 kcal·mol^{-1}·Å^{-1}. Prior to the QM/MM calculations, the MM subsystem was relaxed by performing ~500 steps of energy minimization with the AMBER8 program. Then atoms within 20 Å of the carbonyl carbon (C1) of ATCh were allowed to move, while all the other atoms outside this range were frozen in all QM/MM calculations.

Free Energy Perturbation

After the minimum-energy path was determined by the QM/MM calculations, the free energy changes associated with the QM-MM interactions were determined by using the free energy perturbation (FEP) method.[54] In the FEP calculations, sampling of the MM subsystem was carried out with the QM subsystem frozen at different states along the reaction path. The point charges on the frozen QM atoms used in the FEP calculations were those determined by fitting the electrostatic potential (ESP) for the QM part of the QM/MM single-point calculations. The total free energy difference between the transition state and the reactant was calculated with the same procedure used in our previous work on other reaction systems.[56] The FEP calculations enabled us to more reasonably determine relative free energy changes due to the QM-MM interaction. Technically, the final (relative) free energy determined by the QM/MM-FE calculations is the QM part of the QM/MM energy (excluding the Coulombic interaction energy between the point charges of the MM atoms and the ESP charges of the QM atoms) plus the relative free energy change determined by the FEP calculations. In the FEP calculations, the time step used was 2 fs, and bond lengths involving hydrogen atoms were constrained. In sampling of the MM subsystem by MD simulations, the temperature was maintained at 298.15 K. Each FEP calculation consisted of 50 ps of equilibration and 300 ps of sampling.

The QM/MM-FE calculations were performed on a supercomputer (*e.g*. Lipscomb High Performance Computing cluster with 378 nodes or 4656 processors) at the University of Kentucky Center for Computational Sciences. The other modeling and computations were carried out on SGI Fuel workstations and a 34-processor IBM x335 Linux cluster in our own laboratory.

Results and Discussion

Reaction Pathway for the Hydrolysis of ATCh Catalyzed by BChE

The QM/MM-optimized ES structure for BChE-catalyzed hydrolysis of ATCh is depicted in Figure 1B. In this structure, the internuclear distances between the carbonyl oxygen of ATCh and the NH groups of Gly116, Gly117, and Ala199 are 2.11, 1.88, and 2.34 Å, respectively, showing that the carbonyl oxygen (O1) of ATCh forms hydrogen bonds with the oxyanion hole formed by the backbone NH groups of Gly116, Gly117, and Ala199. The internuclear distance between the carbonyl carbon (C1) of ATCh and the hydroxyl oxygen (O$^{\gamma}$) of Ser198 side chain is ~2.7 Å, indicating an appropriate distance for the Ser198 hydroxyl to start nucleophilic attack on the carbonyl carbon C1 of ATCh. The internuclear distance between the hydroxyl hydrogen (H$^{\gamma}$) of Ser198 and the H$^{\varepsilon}$ of His438 is ~1.7 Å, suggesting that His438, the general base in the BChE catalytic triad, has been positioned well and is ready for facilitating the nucleophilic attack process through accepting a proton from the nucleophile. These values are similar to the corresponding distances in the ES structure for BChE-catalyzed hydrolysis of ACh in our previous study.[47] This is not surprising because the only difference between ACh and ATCh is that the ester oxygen in ACh is replaced by a sulfur atom in ATCh.

Step 1: Nucleophilic Attack on the Carbonyl Carbon by Ser 198—Similar to BChE- catalyzed hydrolysis of ACh from our previous study,[47] the acylation stage of BChE-catalyzed hydrolysis of ATCh is initiated by the nucleophilic attack of the O^{γ} atom of Ser198 side chain on the carbonyl carbon of ATCh. For this reason, the reaction coordinate for the current reaction step was set as $R_{O\gamma\text{-}H\gamma} - R_{Cl\text{-}O\gamma} - R_{N\varepsilon\text{-}H\gamma}$ in which $R_{O\gamma\text{-}H\gamma}$ is the distance between the O^{γ} and H^{γ} atoms of Ser198 side chain, $R_{C\text{-}O\gamma}$ is the distance between the C1 (carbonyl carbon) and O^{γ} atoms, and $R_{N\varepsilon\text{-}H\gamma}$ is the distance between the N^{ε} (on H438 side chain) and H^{γ} atoms. As the O^{γ} atom of Ser198 gradually approaches the C1 atom, the geometry of the reactant (ES), in which the C1 atom is sp^2-hybridized and is in a planar geometry with its three attached groups, gradually changes into a tetrahedral geometry centered at the sp^3-hybridized C1 atom in an intermediate (INT1) through a transition state (TS1). The geometrical parameters in TS1 is similar to the ones in the TS1 structure of BChE-catalyzed hydrolysis of ACh, i.e. the interatomic distances $R_{O\gamma\text{-}H\gamma}$, $R_{C1\text{-}O\gamma}$, and $R_{N\varepsilon\text{-}H\gamma}$ in TS1 are 1.90, 1.64, and 1.07 Å, respectively, close to the corresponding $R_{O\gamma\text{-}H\gamma}$, $R_{C1\text{-}O\gamma}$, and $R_{N\varepsilon\text{-}H\gamma}$ values 1.87, 1.56, and 1.10 Å in the TS1 structure of BChE-catalyzed hydrolysis of ACh. [47] In the intermediate structure of INT1, the optimized internuclear distances $R_{O\gamma\text{-}H\gamma}$, $R_{C1\text{-}O\gamma}$, and $R_{N\varepsilon\text{-}H\gamma}$ are 1.88, 1.53, and 1.04 Å, respectively, indicating that the Ser198 has transferred H^{γ} to the N^{ε} atom of His438. Meanwhile, the optimized C1-S distance between the S atom and the carbonyl carbon is 2.12 Å (Figure 1D), showing that the C1-S bond has been greatly weakened during the nucleophilic attack step.

Step 2: Dissociation of the Thiocholine Ester—In this reaction step, the thiocholine moiety of ATCh gradually departs from the acetyl group in which the thiocholine thioester bond C1-S is broken. Meanwhile, the proton (H^{γ}) attached to the N^{ε} atom of the His438 side chain transfers to thiocholine sulfur atom (S) of ATCh. The changes of the distances $R_{C1\text{-}S}$, $R_{S\text{-}H\gamma}$, and $R_{N\varepsilon\text{-}H\gamma}$ reflect the nature of the dissociation process. Thus, the reaction coordinate for the current reaction step was chosen to be $R_{C1\text{-}S} + R_{N\varepsilon\text{-}H\gamma} - R_{S\text{-}H\gamma}$.

In the geometry of INT1 in which the serine hydroxyl proton (H^{γ}) has been transferred to the N^{ε} atom of His438 in reaction step 1, the optimized distance ($R_{O\gamma\text{-}H\gamma}$) is 1.88 Å, suggesting the interaction between the Ser198 terminal oxygen and the protonated His438 side chain is quite strong. At the same time, the distance ($R_{S\text{-}H\gamma}$) between H^{γ} (attached to His438) and the leaving atom S to which H^{γ} is about to be transferred is as long as 3.15 Å, indicating that the H^{γ} atom is not in the appropriate place to protonate the leaving S atom of ATCh. The $R_{S\text{-}H\gamma}$ value of 3.15 Å in INT1 is larger than the corresponding $R_{O2\text{-}H\gamma}$ value of 2.32 Å in the INT1 structure of BChE- catalyzed hydrolysis of ACh,[47] which is partly due to the fact that the atomic radius of the sulfur atom (0.88 Å) is larger than that of the oxygen atom (0.48 Å). Because of the same reason, in the subsequent step the optimized interatomic distances involving the sulfur atom will be slightly longer than the corresponding ones obtained from the study on ACh hydrolysis catalyzed by BChE.

In changing from INT1 to TS2, there are two major types of structural changes. One is the gradual breaking of the covalent bond C1-S ($R_{C1\text{-}S}$ is 2.12 Å in INT1 and 2.87 Å in TS2). The other is the formation of a hydrogen bond ($N^{\varepsilon}\text{-}H^{\gamma}\cdots S$) indicated by the shorter and shorter distance $R_{S\text{-}H\gamma}$ in going from INT1 to TS2 (3.15 Å in INT1 and 1.65 Å in TS2). In the meantime, the hydrogen bond $N^{\varepsilon}\text{-}H^{\gamma}\cdots O^{\gamma}$ involving the transferring proton (H^{γ}) and the O^{γ} atom of Ser198 becomes progressively weaker ($R_{O\gamma\text{-}H\gamma}$ is 1.88 Å in INT1 and 2.72 Å in TS2), which is reasonable as the transferring proton (H^{γ}) is about to be transferred to the leaving sulfur atom (S) in the current reaction step.

Step 3: Nucleophilic Attack on the Carbonyl Carbon by a Water Molecule—The thiocholine was removed from the above-discussed QM/MM-optimized geometry of INT2 to construct the structure of INT2′, which was then relaxed by performing MD simulation.

The deacylation stage in BChE-catalyzed hydrolysis of ATCh is the same as that in BChE-catalyzed hydrolysis of ACh since the leaving group choline/thiocholine has been released after the acylation stage. A water molecule close to the carbonyl carbon (C1) of the substrate was selected as the nucleophile and was treated by the QM method. Similar to that in the acylation stage, the carbonyl oxygen of the substrate is also stabilized by the oxyanion hole. As shown in Figure 2B, two strong hydrogen bonds are formed between the carbonyl oxygen (O1) of ATCh and the oxyanion hole in INT2′.

The current nucleophilic attacking process involves the breaking of the O^{ω}-H^{ω} bond and the formation of both C1-O^{ω} and N^{ε}-H^{ω} bonds (see Figure 2B). Thus, the distances $R_{O\omega\text{-}H\omega}$, $R_{C1\text{-}O\omega}$, and $R_{N\varepsilon\text{-}H\omega}$ were chosen to establish the reaction coordinate as $R_{O\omega\text{-}H\omega} - R_{C1\text{-}O\omega} + R_{N\varepsilon\text{-}H\omega}$ for the current reaction step. In proceeding from INT2′ to INT3 through the transition state TS2 (Figure 2), the coplanar geometry changes into tetrahedral centering on the sp^3-hybridized carbonyl carbon (C1) atom as the nucleophilic water gradually approaches the C1 atom with a spontaneous proton (H^{ω}) transferring from the O^{ω} atom of the nucleophilic water to the N^{ε} atom of the His438 side chain. The QM/MM-optimized geometry of INT3 shows that the nucleophilic attack process is completed with water dissociating into hydroxide ion attaching to the C1 atom and a proton (H^{ω}) attaching to the N^{ε} atom.

Step 4: Dissociation between the Acetyl Group and Ser198 of BChE—The proton transfer between the N^{ε} atom of His438 side chain and the O^{γ} atom of Ser198 side chain and the breaking of the covalent bond C1-O^{γ} are involved in the dissociation of acetyl-enzyme. The changes of the distances $R_{C1\text{-}O\gamma}$, $R_{O\gamma\text{-}H\omega}$, and $R_{N\varepsilon\text{-}H\omega}$ reflect the nature of reaction step 3. Thus, the reaction coordinate for the current reaction step was expressed as $R_{C1\text{-}O\gamma} - R_{N\varepsilon\text{-}H\omega} - R_{O\gamma\text{-}H\omega}$. In reaction step 3, the C-O covalent bond is broken and a proton is transferred from the N^{ε} atom of His438 to the oxygen atom of the broken C-O covalent bond. As shown in Figure 2, during the breaking of the C1-O^{γ} covalent bond, the distance between the O^{γ} and H^{ω} atoms becomes closer and closer, illustrating a spontaneous proton transfer from the N^{ε} atom of His438 side chain to the O^{γ} atom of Ser198.

Energetics and Kinetic Parameters

Depicted in Figures 3 are the free energy profiles for BChE-catalyzed hydrolysis of ATCh, determined by the QM/MM-FE calculations at the MP2/6-31+G*:AMBER level excluding the zero-point and thermal corrections for the QM subsystem. The values given in parentheses are the corresponding relative free energies including the zero-point and thermal corrections for the QM subsystem.

1. Rate-determining step—As shown in Figure 3A, with the zero-point and thermal corrections for the QM subsystem, the free energy barriers calculated for the first and second step (acylation) of BChE-catalyzed hydrolysis of ATCh are 11.4 and 6.7 kcal/mol, respectively. Although the free energy barrier for the first reaction step is higher than that for the second reaction step, the relative free energy of TS2 is higher than that of TS1, indicating that the calculated overall free energy barrier for the acylation is the free energy change from ES to TS2, which is 13.6 kcal/mol. Similarly, in the deacylation stage of BChE-catalyzed hydrolysis of ATCh, the free energy barrier (9.5 kcal/mol) calculated for the third reaction step is higher than that (4.8 kcal/mol) calculated for the fourth reaction step, but the relative free energy of TS4 is higher than that of TS3, implying that the calculated overall free energy barrier for the deacylation is the free energy change from INT2′ to TS3, which is 9.7 kcal/mol. Apparently, the acylation stage with the overall free energy barrier of 13.6 kcal/mol, which is the free energy change from ES to TS2, is rate-determining for BChE-catalyzed hydrolysis of ATCh. The conclusion is in consistent with

the previous study on BChE-catalyzed hydrolysis of ACh, in which the acylation reactions was found to be rate-determining.[47]

In fact, the experimental catalytic rate constant for BChE-catalyzed hydrolysis of ATCh was reported to be 2.02×10^4 min^{-1}.[2] According to the conventional transition state theory (CTST),[63] a rate constants of 2.02×10^4 min^{-1} is associated with an activation free energy of 14.0 kcal/mol. The predicted free energy barrier of 13.6 kcal/mol is in good agreement with the experimentally-derived activation free energy of 14.0 kcal/mol.

2. Substrate activation effect—As mentioned above, the hydrolysis of ATCh by BChE can be accelerated by excessive substrate ATCh in the reaction system. Masson *et al*. investigated this substrate activation phenomenon by site-directed mutagenesis and steady-state kinetic experiment.[42] They have found that the Asp70 residue, which is located at the PAS of BChE, is the only residue which is important for this function. In substrate activation phase, an additional substrate molecule will transiently bind to the Asp70 residue. They further proposed a binding mode of this additional substrate molecule with the PAS by molecular docking.[42] Based on the binding mode described by Masson *et al*., we placed an ATCh molecule in the PAS of BChE ES complex structure. The position and orientation of this molecule were further refined by performing ~500 steps of energy minimization using the AMBER8 program. In the optimized structure (see Figure 4), the positively charged $-N^+(CH_3)_3$ moiety of this molecule is ~4.6 Å away from the carboxylate oxygen of Asp70, indication a strong electrostatic attraction interaction between the ATCh molecule at PAS and the Asp70. On the other hand, the substrate molecule at PAS is more than 11 Å away from the catalytic site (QM subsystem of BChE, where the hydrolysis reaction takes place, implying that the substrate molecule at PAS will not be directly involved in the reaction pathway. Furthermore, since the substrate molecule at PAS is far away from the QM subsystem, the van de Waal interactions between the additional substrate molecule at PAS and the active site of BChE is negligible. The free energy barrier of ATCh hydrolysis by BChE could only be affected by the long-range electrostatic interactions between the substrate molecule at PAS and the QM subsystem. Thus, the effects of the electrostatic interaction between the QM subsystem and the substrate molecule at PAS were estimated by performing the QM calculations on the QM subsystem (at each state during the reaction process) in the presence and absence of the point charges of the atoms in the substrate molecule at PAS. As shown in Table 1, the estimated shifts of the relative free energies due to the electrostatic effect of the additional ATCh molecule at PAS for TS1, INT1, TS2, and INT2 during the acylation stage are −1.4, −2.5, −1.7, and −0.5 kcal/mol, respectively. The estimated shifts of the relative free energies for TS3, INT3, TS4, and PD during the deacylation stage are −0.1, −0.1, 0.1, and 0.6 kcal/mol, respectively. Further, replacing the point charges of the atoms in the ATCh molecule at PAS with a single unit positive (+1) charge in the calculations, the resulted relative free energies are very close to the corresponding ones obtained with the point charges of the atoms in the ATCh molecule at PAS (see Table 1). Hence, we may conclude that the positive charge at the $-N^+(CH_3)_3$ moiety of the ATCh molecule at PAS plays a key role for the substrate activation phenomenon observed in the BChE-catalyzed hydrolysis of ATCh. The data in Table 1 indicate that, at the substrate activation phase, the acylation of BChE is still rate-determining, with an overall free energy barrier of 11.9 kcal/mol. The calculated shift of the overall free energy barrier (from 13.6 kcal/mol to 11.9 kcal/mol) is qualitatively consistent with the experimentally observed substrate activation that the excessive substrate ATCh accelerates the BChE-catalyzed hydrolysis of ATCh. According to the reported experimental kinetic data,[2] the experimental activation free energy decreased from of 14.0 kcal/mol for the regular hydrolysis phase to 13.5 kcal/mol for the substrate activation phase. Our theoretical calculations overestimated the substrate activation effect, which is likely due to the imperfect computational model used in the present study. Nevertheless, our calculated

results have clearly demonstrated that the additional ATCh molecule at the PAS site is responsible for the substrate activation phenomenon of ATCh hydrolysis by BChE.

Conclusion

In this work, we employed pseudobond first-principles QM/MM-FE approach to study the reaction pathway for BChE-catalyzed hydrolysis of ATCh and the corresponding free energy profiles. The computational results demonstrate that ATCh hydrolysis catalyzed by BChE consists of two major reaction stages, *i.e*. acylation and deacylation of BChE. The acylation with ATCh includes two reaction steps including the nucleophilic attack on the carbonyl carbon of ATCh and the dissociation of thiocholine ester. The deacylation stage includes the nucleophilic attack of a water molecule on the carboxyl carbon of substrate, followed by the dissociation between the carbonyl carbon of substrate and hydroxyl oxygen of Ser198 side chain. The computationally determined free energy profiles indicate that the acylation is rate-determining for BChE-catalyzed hydrolysis of ATCh. In substrate activation phase, an additional ATCh molecule will bind with the PAS of BChE. Our QM calculations demonstrate that the positive charge of the ATCh at PAS will reduce the free energy barrier of the ATCh hydrolysis by ~1.7 kcal/mol and thus lead to the substrate activation phenomenon of ATCh hydrolysis by BChE. The overall free energy barriers calculated for BChE-catalyzed hydrolysis of ATCh at the regular hydrolysis phase and the substrate activation phase are ~13.6 and ~11.9 kcal/mol, respectively, which are in reasonable agreement with the corresponding experimentally-derived activation free energies of 14.0 kcal/mol (for regular hydrolysis phase) and 13.5 kcal/mol (for substrate activation phase).

Acknowledgments

The entire work was performed at University of Kentucky. The authors also acknowledge the Center for Computational Sciences (CCS) at University of Kentucky for supercomputing time. Chen and Liu worked in Zhan's laboratory for this project at University of Kentucky.

Funding. This work was supported in part by NIH (grants R01 DA025100 and R01 DA013930 to Zhan).

References

1. Fuxreiter M, Warshel A. Origin of the catalytic power of acetylcholinesterase: Computer simulation studies. J. Am. Chem. Soc. 1998; 120:183–194.
2. Boeck AT, Schopfer LM, Lockridge O. DNA sequence of butyrylcholinesterase from the rat: expression of the protein and characterization of the properties of rat butyrylcholinesterase. Biochem. Pharmacol. 2002; 63:2101–2110. [PubMed: 12110369]
3. Zhan CG, Gao DQ. Catalytic mechanism and energy barriers for butyrylcholinesterase-catalyzed hydrolysis of cocaine. Biophys. J. 2005; 89:3863–3872. [PubMed: 16319079]
4. Masson P, Froment MT, Gillon E, Nachon F, Lockridge O, Schopfer LM. Kinetic analysis of effector modulation of butyrylcholinesterase-catalysed hydrolysis of acetanilides and homologous esters. FEBS J. 2008; 275:2617–2631. [PubMed: 18422653]
5. Mesulam MM, Guillozet A, Shaw P, Levey A, Duysen EG, Lockridge O. Acetylcholinesterase knockouts establish central cholinergic pathways and can use butyrylcholinesterase to hydrolyze acetylcholine. Neuroscience. 2002; 110:627–639. [PubMed: 11934471]
6. Mesulam M, Guillozet A, Shaw P, Quinn B. Widely spread butyrylcholinesterase can hydrolyze acetylcholine in the normal and Alzheimer brain. Neurobiol. Dis. 2002; 9:88–93. [PubMed: 11848688]
7. Millard CB, Lockridge O, Broomfield CA. Design and expression of organophosphorus acid anhydride hydrolase activity in human butyrylcholinesterase. Biochemistry. 1995; 34:15925–15933. [PubMed: 8519749]

8. Lockridge O, Blong RM, Masson P, Froment MT, Millard CB, Broomfield CA. A single amino acid substitution, Gly117His, confers phosphotriesterase (organophosphorus acid anhydride hydrolase) activity on human butyrylcholinesterase. Biochemistry. 1997; 36:786–795. [PubMed: 9020776]
9. Pan YM, Gao DQ, Yang WC, Cho H, Yang GF, Tai HH, Zhan CG. Computational redesign of human butyrylcholinesterase for anticocaine medication. Proc. Natl. Acad. Sci. U. S. A. 2005; 102:16656–16661. [PubMed: 16275916]
10. Zhan CG, Zheng F, Landry DW. Fundamental reaction mechanism for cocaine hydrolysis in human butyrylcholinesterase. J. Am. Chem. Soc. 2003; 125:2462–2474. [PubMed: 12603134]
11. Gao DQ, Cho H, Yang WC, Pan YM, Yang GF, Tai HH, Zhan CG. Computational design of a human butyrylcholinesterase mutant for accelerating cocaine hydrolysis based on the transition-state simulation. Angew. Chem. Int. Edit. 2006; 45:653–657.
12. Zheng F, Yang WC, Ko MC, Liu JJ, Cho H, Gao DQ, Tong M, Tai HH, Woods JH, Zhan CG. Most efficient cocaine hydrolase designed by virtual screening of transition states. J. Am. Chem. Soc. 2008; 130:12148–12155. [PubMed: 18710224]
13. Zheng F, Zhan C-G. Rational design of an enzyme mutant for anti-cocaine therapeutics. J. Comput. Aid. Mol. Des. 2008; 22:661–671.
14. Zheng F, Zhan C-G. Structure-and-mechanism-based design and discovery of therapeutics for cocaine overdose and addiction. Org. Biomol. Chem. 2008; 6:836–843. [PubMed: 18292872]
15. Gao DQ, Zhan CG. Modeling effects of oxyanion hole on the ester hydrolysis catalyzed by human cholinesterases. J. Phys. Chem. B. 2005; 109:23070–23076. [PubMed: 16854005]
16. Zhan C-G. Novel pharmacological approaches to treatment of drug overdose and addiction. Expert Rev. Clin. Pharmacol. 2009; 2:1–4. [PubMed: 21072135]
17. Yang W, Pan Y, Zheng F, Cho H, Tai H-H, Zhan C-G. Free-Energy Perturbation Simulation on Transition States and Redesign of Butyrylcholinesterase. Biophys. J. 2009; 96:1931–1938. [PubMed: 19254552]
18. Pan YM, Gao DQ, Yang WC, Cho H, Zhan CG. Free energy perturbation (FEP) simulation on the transition states of cocaine hydrolysis catalyzed by human butyrylcholinesterase and its mutants. J. Am. Chem. Soc. 2007; 129:13537–13543. [PubMed: 17927177]
19. Hamza A, Cho H, Tai H-H, Zhan C-G. Molecular Dynamics Simulation of Cocaine Binding with Human Butyrylcholinesterase and Its Mutants. J. Phys. Chem. B. 2005; 109:4776–4782. [PubMed: 16851561]
20. Gao DQ, Zhan C-G. Modeling evolution of hydrogen bonding and stabilization of transition states in the process of cocaine hydrolysis catalyzed by human butyrylcholinesterase. Proteins. 2006; 62:99–110. [PubMed: 16288482]
21. Yang W, Xue L, Fang L, Chen X, Zhan C-G. Characterization of a high-activity mutant of human butyrylcholinesterase against (-)-cocaine. Chem.-Biol. Interact. 2010; 187:148–152. [PubMed: 20060817]
22. Yang W, Pan Y, Fang L, Gao D, Zheng F, Zhan C-G. Free Energy Perturbation Simulation on Transition States and High-Activity Mutants of Human Butyrylcholinesterase for (-)-Cocaine Hydrolysis. J. Phys. Chem. B. 2010; 114:10889–10896. [PubMed: 20677742]
23. Brimijoin S, Gao Y, Anker JJ, Gliddon LA, LaFleur D, Shah R, Zhao QH, Singh M, Carroll ME. A cocaine hydrolase engineered from human butyrylcholinesterase selectively blocks cocaine toxicity and reinstatement of drug seeking in rats. Neuropsychopharmacology. 2008; 33:2715–2725. [PubMed: 18199998]
24. Decker M. Novel inhibitors of acetyl- and butyrylcholinesterase derived from the alkaloids dehydroevodiamine and rutaecarpine. Eur. J. Med. Chem. 2005; 40:305–313. [PubMed: 15725500]
25. Sussman JL, Harel M, Frolow F, Oefner C, Goldman A, Toker L, Silman I. Atomic-Structure of Acetylcholinesterase from Torpedo-Californica - a Prototypic Acetylcholine-Binding Protein. Science. 1991; 253:872–879. [PubMed: 1678899]
26. Saxena A, Redman AMG, Jiang XL, Lockridge O, Doctor BP. Differences in active site gorge dimensions of cholinesterases revealed by binding of inhibitors to human butyrylcholinesterase. Biochemistry. 1997; 36:14642–14651. [PubMed: 9398183]

27. Wlodek ST, Antosiewicz J, Briggs JM. On the mechanism of acetylcholinesterase action: The electrostatically induced acceleration of the catalytic acylation step. J. Am. Chem. Soc. 1997; 119:8159–8165.
28. Wang QM, Jiang HL, Chen JZ, Chen KX, Ji RY. On the possible reaction pathway for the acylation of AChE-catalyzed hydrolysis of ACh: Semiempirical quantum chemical study. Int. J. Quantum Chem. 1998; 70:515–525.
29. Vagedes P, Rabenstein B, Aqvist J, Marelius J, Knapp EW. The deacylation step of acetylcholinesterase: Computer simulation studies. J. Am. Chem. Soc. 2000; 122:12254–12262.
30. Zhang YK, Kua J, McCammon JA. Role of the catalytic triad and oxyanion hole in acetylcholinesterase catalysis: An ab initio QM/MM study. J. Am. Chem. Soc. 2002; 124:10572–10577. [PubMed: 12197759]
31. Manojkumar TK, Cui CZ, Kim KS. Theoretical insights into the mechanism of acetylcholinesterase-catalyzed acylation of acetylcholine. J. Comput. Chem. 2005; 26:606–611. [PubMed: 15739192]
32. Suarez D, Field MJ. Molecular dynamics simulations of human butyrylcholinesterase. Proteins. 2005; 59:104–117. [PubMed: 15696543]
33. Tachikawa H, Igarashi M, Nishihira J, Ishibashi T. Ab initio model study on acetylcholinesterase catalysis: potential energy surfaces of the proton transfer reactions. J. Photochem. Photobiol., B. 2005; 79:11–23. [PubMed: 15792875]
34. Sant'Anna CMR, Viana AD, do Nascimento NM. A semiempirical study of acetylcholine hydrolysis catalyzed by Drosophila melanogaster acetylcholinesterase. Bioorg. Chem. 2006; 34:77–89. [PubMed: 16540146]
35. Suarez D, Diaz N, Fontecilla-Camps J, Field MJ. A computational study of the deacylation mechanism of human butyrylcholinesterase. Biochemistry. 2006; 45:7529–7543. [PubMed: 16768449]
36. Zhou Y, Wang S, Zhang Y. Catalytic Reaction Mechanism of Acetylcholinesterase Determined by Born-Oppenheimer Ab Initio QM/MM Molecular Dynamics Simulations. J. Phys. Chem. B. 2010; 114:8817–8825. [PubMed: 20550161]
37. Froede HC, Wilson IB. Direct Determination of Acetyl-Enzyme Intermediate in the Acetylcholinesterase-Catalyzed Hydrolysis of Acetylcholine and Acetylthiocholine. J. Biol. Chem. 1984; 259:1010–1013.
38. Nemukhin AV, Lushchekina SV, Bochenkova AV, Golubeva AA, Varfolomeev SD. Characterization of a complete cycle of acetylcholinesterase catalysis by ab initio QM/MM modeling. J. Mol. Model. 2008; 14:409–416. [PubMed: 18343962]
39. Mesulam M, Guillozet A, Shaw P, Quinn B. Widely spread butyrylcholinesterase can hydrolyze acetylcholine in the normal and Alzheimer brain. Neurobiol. Dis. 2002; 9:88–93. [PubMed: 11848688]
40. Eriksson H, Augustinsson KB. Mechanisitic model for butyrylcholinesterase. Biochim. Biophys. Acta. 1979; 567:161–173. [PubMed: 454620]
41. Komers K, Cegan A, Link M. Kinetics and mechanism of hydrolysis of acetylthiocholine by butyrylcholine esterase. Z. Naturforsch. [C]. 2002; 57:1072–1077.
42. Masson P, Froment MT, Bartels CF, Lockridge O. Asp70 in the peripheral anionic site of human butyrylcholinesterase. Eur. J. Biochem. 1996; 235:36–48. [PubMed: 8631355]
43. Tormos JR, Wiley KL, Seravalli J, Nachon F, Masson P, Nicolet Y, Quinn DM. The reactant state for substrate-activated turnover of acetylthiocholine by butyrylcholinesterase is a tetrahedral intermediate. J. Am. Chem. Soc. 2005; 127:14538–14539. [PubMed: 16231883]
44. Wiley KL, Tormos JR, Quinn DM. A secondary isotope effect study of equine serum butyrylcholinesterase-catalyzed hydrolysis of acetylthiocholine. Chem.-Biol. Interact. 2010; 187:124–127. [PubMed: 20493178]
45. Shafferman A, Velan B, Ordentlich A, Kronman C, Grosfeld H, Leitner M, Flashner Y, Cohen S, Barak D, Ariel N. Substrate-Inhibition of Acetylcholinesterase - Residues Affecting Signal Transduction from the Surface to the Catalytic Center. EMBO J. 1992; 11:3561–3568. [PubMed: 1396557]

46. Gao Y, LaFleur D, Shah R, Zhao QH, Singh M, Brimijoin S. An albumin-butyrylcholinesterase for cocaine toxicity and addiction: Catalytic and pharmacokinetic properties. Chem. -Biol. Interact. 2008; 175:83–87. [PubMed: 18514640]
47. Chen X, Fang L, Liu JJ, Zhan CG. Reaction Pathway and Free Energy Profile for Butyrylcholinesterase-Catalyzed Hydrolysis of Acetylcholine. J. Phys. Chem. B. 2011; 115:1315–1322. [PubMed: 21175195]
48. Eriksson H, Augustinsson KB. Mechanistic Model for Butyrylcholinesterase. Biochim Biophys Acta. 1979; 567:161–173. [PubMed: 454620]
49. Komers K, Cegan A, Link M. Kinetics and mechanism of hydrolysis of acetylthiocholine by butyrylcholine esterase. Z.Naturforsch.(C). 2002; 57:1072–1077. [PubMed: 12562097]
50. Gao Y, LaFleur D, Shah R, Zhao QH, Singh M, Brimijoin S. An albumin-butyrylcholinesterase for cocaine toxicity and addiction: Catalytic and pharmacokinetic properties. Chem. Biol. Interact. 2008; 175:83–87. [PubMed: 18514640]
51. Zhang YK. Improved pseudobonds for combined ab initio quantum mechanical/molecular mechanical methods. J. Chem. Phys. 2005; 122:024114. [PubMed: 15638579]
52. Zhang YK, Lee TS, Yang WT. A pseudobond approach to combining quantum mechanical and molecular mechanical methods. J. Chem. Phys. 1999; 110:46–54.
53. Hu P, Zhang YK. Catalytic mechanism and product specificity of the histone lysine methyltransferase SET7/9: An ab initio QM/MM-FE study with multiple initial structures. J. Am. Chem. Soc. 2006; 128:1272–1278. [PubMed: 16433545]
54. Zhang YK, Liu HY, Yang WT. Free energy calculation on enzyme reactions with an efficient iterative procedure to determine minimum energy paths on a combined ab initio QM/MM potential energy surface. J. Chem. Phys. 2000; 112:3483–3492.
55. Zhang YK. Pseudobond ab initio QM/MM approach and its applications to enzyme reactions. Theor. Chem. Acc. 2006; 116:43–50.
56. Liu JJ, Hamza A, Zhan CG. Fundamental Reaction Mechanism and Free Energy Profile for (-)-Cocaine Hydrolysis Catalyzed by Cocaine Esterase. J. Am. Chem. Soc. 2009; 131:11964–11975. [PubMed: 19642701]
57. Liu JJ, Zhang YK, Zhan CG. Reaction Pathway and Free-Energy Barrier for Reactivation of Dimethylphosphoryl-Inhibited Human Acetylcholinesterase. J. Phys. Chem. B. 2009; 113:16226–16236. [PubMed: 19924840]
58. Poyner RR, Larsen TM, Wong SW, Reed GH. Functional and structural changes due to a serine to alanine mutation in the active-site flap of enolase. Arch. Biochem. Biophys. 2002; 401:155–163. [PubMed: 12054465]
59. Cisneros GA, Wang M, Silinski P, Fitzgerald MC, Yang WT. The protein backbone makes important contributions to 4-oxalocrotonate tautomerase enzyme catalysis: Understanding from theory and experiment. Biochemistry. 2004; 43:6885–6892. [PubMed: 15170325]
60. Metanis N, Brik A, Dawson PE, Keinan E. Electrostatic interactions dominate the catalytic contribution of Arg39 in 4-oxalocrotonate tautomerase. J. Am. Chem. Soc. 2004; 126:12726–12727. [PubMed: 15469238]
61. Frisch, MJ.; Trucks, GW.; Schlegel, HB.; Scuseria, GE.; Robb, MA.; Cheeseman, JR.; Montgomery, J.; J, A.; Vreven, T.; Kudin, KN.; Burant, JC.; Millam, JM.; Iyengar, SS.; Tomasi, J.; Barone, V.; Mennucci, B.; Cossi, M.; Scalmani, G.; Rega, N.; Petersson, GA.; Nakatsuji, H.; Hada, M.; Ehara, M.; Toyota, K.; Fukuda, R.; Hasegawa, J.; Ishida, M.; Nakajima, T.; Honda, Y.; Kitao, O.; Nakai, H.; Klene, M.; Li, X.; Knox, JE.; Hratchian, HP.; Cross, JB.; Bakken, V.; Adamo, C.; Jaramillo, J.; Gomperts, R.; Stratmann, RE.; Yazyev, O.; Austin, AJ.; Cammi, R.; Pomelli, C.; Ochterski, JW.; Ayala, PY.; Morokuma, K.; Voth, GA.; Salvador, P.; Dannenberg, JJ.; Zakrzewski, VG.; Dapprich, S.; Daniels, AD.; Strain, MC.; Farkas, O.; Malick, DK.; Rabuck, AD.; Raghavachari, K.; Foresman, JB.; Ortiz, JV.; Cui, Q.; Baboul, AG.; Clifford, S.; Cioslowski, J.; Stefanov, BB.; Liu, G.; Liashenko, A.; Piskorz, P.; Komaromi, I.; Martin, RL.; Fox, DJ.; Keith, T.; Al-Laham, MA.; Peng, CY.; Nanayakkara, A.; Challacombe, M.; Gill, PMW.; Johnson, B.; Chen, W.; Wong, MW.; Gonzalez, C.; Pople, JA. Gaussian 03, Revision C.02. Gaussian, Inc.; Wallingford, CT: 2004.

62. Case, DA.; Darden, TA.; T, E.; Cheatham, I.; Simmerling, CL.; Wang, J.; Duke, RE.; Luo, R.; Merz, KM.; Wang, B.; Pearlman, DA.; Crowley, M.; Brozell, S.; Tsui, V.; Gohlke, H.; Mongan, J.; Hornak, V.; Cui, G.; Beroza, P.; Schafmeister, C.; Caldwell, JW.; Ross, WS.; Kollman, PA. AMBER8. University of California; San Francisco: 2004.

63. Alvarez-Idaboy JR, Galano A, Bravo-Perez G, Ruiz ME. Rate constant dependence on the size of aldehydes in the NO3+ aldehydes reaction. An explanation via quantum chemical calculations and CTST. J Am Chem Soc. 2001; 123:8387–8395. [PubMed: 11516288]

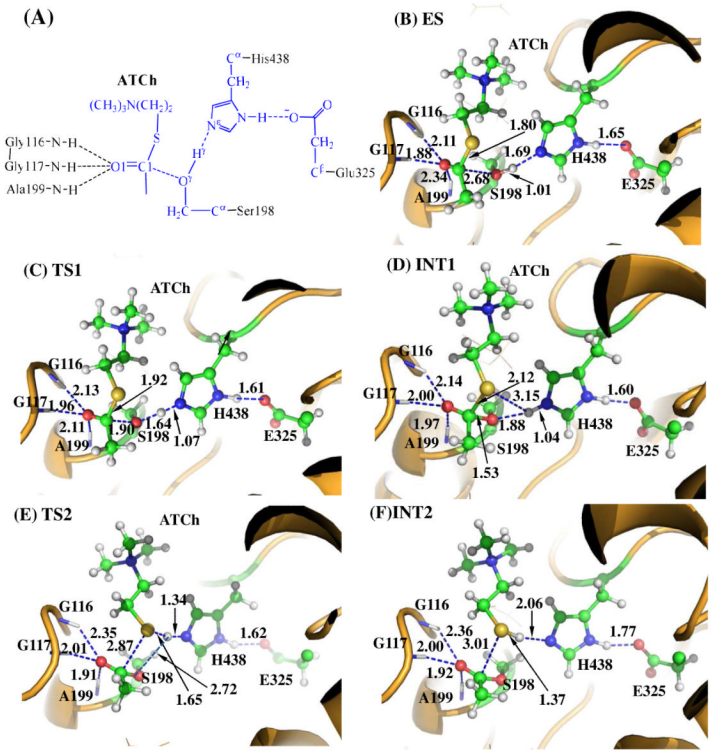

Figure 1.

Key states for the acylation reaction stage of BChE-catalyzed ATCh hydrolysis. The geometries were optimized at the QM/MM(B3LYP/6-31+G*:AMBER) level. The key distances in the figure are in Å. Carbon, oxygen, nitrogen, sulfur, and hydrogen atoms are colored in green, red, blue, yellow, and white, respectively. The backbone of the protein is rendered in orange. The QM atoms are represented as balls and sticks and the surrounding residues are rendered as sticks or lines. The figures below are represented using the same method.

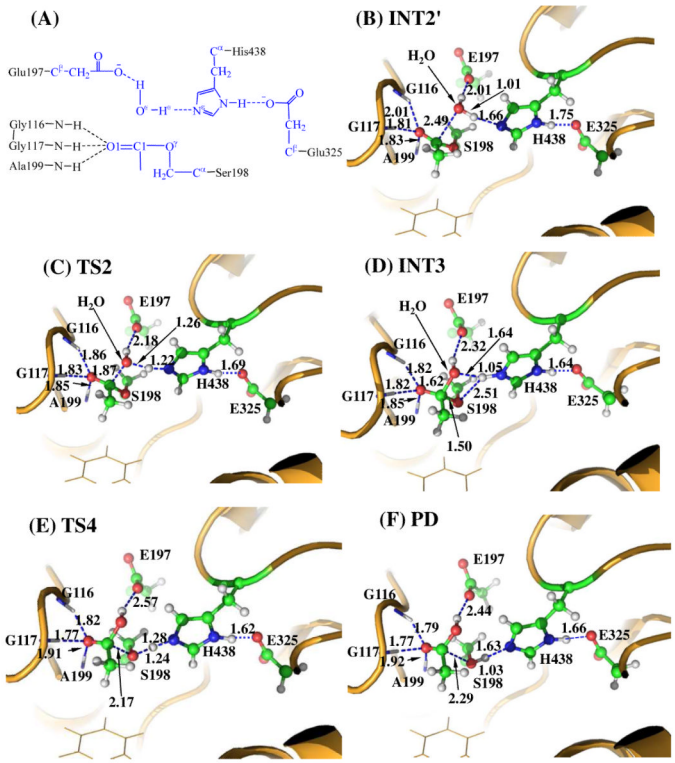

Figure 2.

Key states for the deacylation reaction of BChE-catalyzed ATCh hydrolysis. The geometries were optimized at QM/MM(B3LYP/6-31+G*:AMBER) level. See caption of Figure 1 for the color codes for different types of atoms.

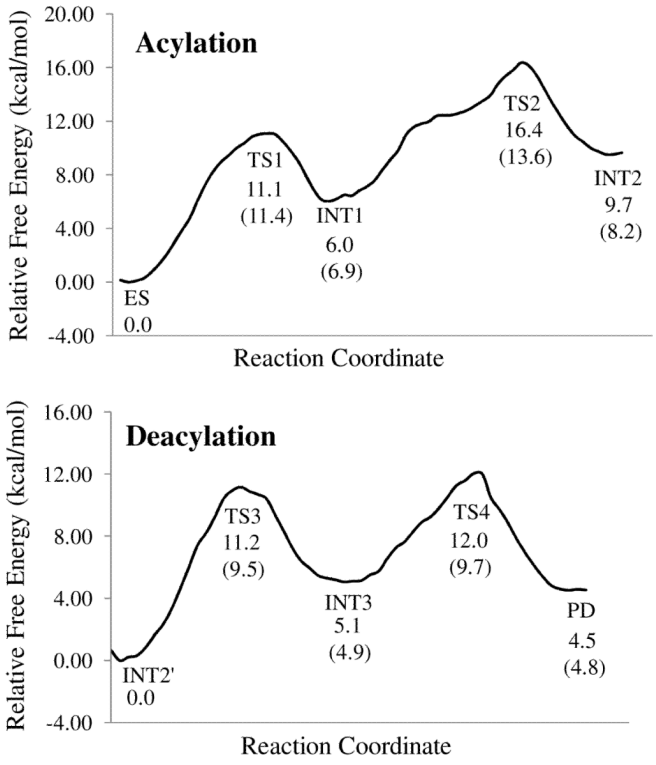

Figure 3.

Free energy profiles for the acylation and deacylation stages of BChE-catalyzed hydrolysis of ATCh. The relative free energies were determined by the QM/MM-FE calculations at the MP2/6-31+G*:AMBER level, excluding the zero-point and thermal corrections for the QM system. Values in the parenthesis are relative free energies including the zero-point and thermal corrections for the QM subsystem.

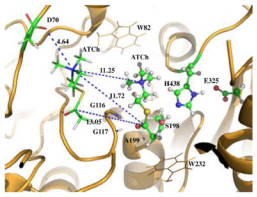

Figure 4.

In substrate activate phase, an additional substrate ATCh molecule binds with the peripheral anionic site of BChE and interacts with the QM part of BChE by electrostatic interaction. Atoms of the QM part are rendered in balls and sticks. Atoms of the additional ATCh and Asp70 (D70) in the peripheral anionic site are rendered in sticks. Other atoms of BChE are rendered in cartoon of lines. See caption of Figure 1 for the color codes for different types of atoms.

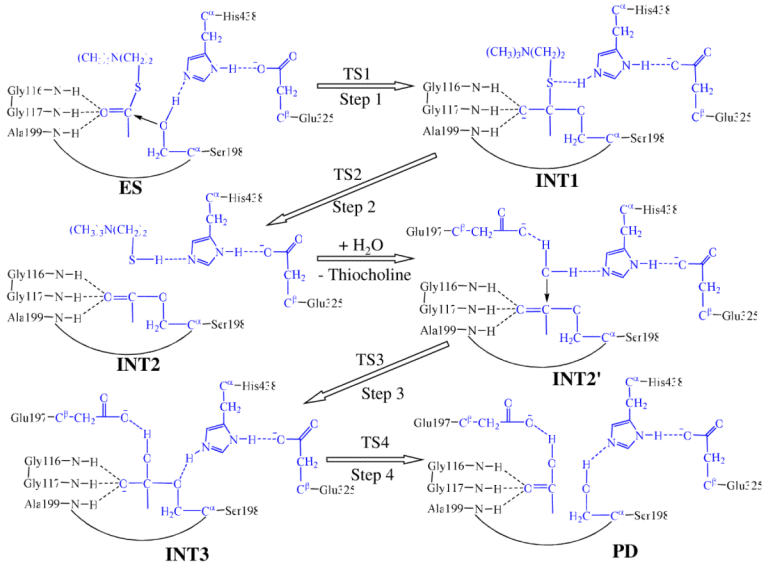

Scheme 1.
Proposed catalytic mechanism for BChE-catalyzed hydrolysis of acetylthiocholine

Table 1

Relative free energies (in kcal/mol) calculated with or without the considering the effect of the additional ATCh molecule at PAS of BChE.

Structure	ΔG (no ATCh at PAS)[a]	ΔG (with ATCh at PAS)[b]	ΔG (with +1 charge at PAS)[c]
Acylation Stage			
ES	0.0	0.0	0.0
TS1	11.4	10.0	10.1
INT1	6.9	4.4	4.5
TS2	13.6	11.9	11.7
INT2	8.2	7.7	7.8
Deacylation stage			
INT2′	0.0	0.0	0.0
TS3	9.5	9.4	9.4
INT3	4.9	4.8	4.8
TS4	9.7	9.8	9.8
PD	4.8	5.4	5.4

[a] Relative Gibbs free energies calculated without considering the effect of the additional ATCh molecule at PAS of BChE.

[b] Relative Gibbs free energies calculated by accounting for the electrostatic effect of the point charges of the atoms in the additional ATCh molecule at PAS.

[c] Relative Gibbs free energies calculated by replacing the point charges of the ATCh at PAS with a single unit positive (+1) charge.